Bioinspired Gradients

Deutsche Ausgabe: DOI: 10.1002/ange.201511512
Internationale Ausgabe: DOI: 10.1002/anie.201511512

Bioinspired Mechanical Gradients in Cellulose Nanofibril/Polymer Nanopapers

*Baochun Wang, Alejandro J. Benitez, Francisco Lossada, Remi Merindol, and Andreas Walther**

Abstract: *Mechanical gradients are important as tough joints, for strain field engineering in printable electronics, for actuators, and for biological studies, yet they are difficult to prepare and quantitatively characterize. We demonstrate the additive fabrication of gradient bioinspired nanocomposites based on stiff, renewable cellulose nanofibrils that are bottom-up toughened via a tailor-made copolymer. Direct filament writing of different nanocomposite hydrogels in patterns, and subsequent healing of the filaments into continuous films while drying leads to a variety of linear, parabolic and striped bulk gradients. In situ digital image correlation under tensile deformation reveals important differences in the strain fields regarding asymmetry and step heights of the patterns. We envisage that merging top-down and bottom-up structuring of nanocellulose hybrids opens avenues for aperiodic and multi-scale, bioinspired nanocomposites with optimized combinations of stiffness and toughness.*

Mechanical gradients are ubiquitous in nature, such as in the attachment of ligaments to bones or in the squid beak.[1] They serve stress delocalization and optimize mechanical properties with regard to toughness, stiffness and abrasion resistance.[2] They inspire future synthetic materials for structural as well as functional applications. For structural materials it is for instance desirable to have tough joints between regions of high elasticity and those of high stiffness. In hydrogels, the crosslinking density and mechanical properties provide instructive cues for cell proliferation, cell migration and stem cell differentiation.[3]

Gradient materials can be distinguished into layered, (sandwich-type) and lateral ones. Sandwich-type gradients can be realized with classical engineering approaches using stacking and fusion of mechanically different materials, or via sequential photo-crosslinking of deposited layers.[4] Although such strategies are rather established, recent examples highlight their importance to delocalize strain through layers of continuously increasing stiffness, or for actuation of bilayer hydrogel stripes.[4a,b] Higher functionality may be accessible by doping functional nanoparticles or orienting them in external fields.[5]

In contrast to sandwich gradients, approaches towards lateral ones are much more scarce and mostly focus on simple, linear gradients of polymer systems.[4c] For instance, Claussen et al. reported linear gradients composed of di- or trifunctional acrylates (as crosslinkers) and thio-siloxane (as prepolymer) via the controlled mixing and lateral deposition using two syringes filled with prepolymer and crosslinker and by changing their mixing ratios during extrusion.[6] The approach was extended to gradient biopolymer gels and films based on fibroin and gelatin.[7]

Typically, the mechanical properties are only described for selected positions of the gradient ex situ by cutting samples perpendicularly, or by replicating mixtures reminiscent of the composition of the gradient. However, this does not give sufficient information on the real strain fields in situ, which needs to be understood for actual materials design.

Towards bioactive gradients, Diederich et al. reported linear gradient polyacrylamide hydrogels to control the kinetics of cell spreading. For instance fibroblasts transformed quickly from a rounded to a spread, adherent morphology on hard areas, while they retained rounded morphologies on soft parts.[8] Hence, this highlights the importance of encoding gradients for biomaterial applications, and for understanding and controlling the biointerface between materials and tissues.

In contrast to classical polymer materials or well-developed hydrogels, we will focus our attention on highly reinforced, bioinspired nanocomposites (nanopapers) formed by emerging and sustainable cellulose nanofibrils (CNF). CNFs are well-defined bionanoparticles with a few nanometers in diameter and several micrometers in length.[9] They are often extracted from wood, and retain the highly crystalline and extremely stiff native character of cellulose I ($E_{\text{cellulose-I}} \approx 145$ GPa).[10] Thus, they hold great promise for sustainable high-performance structural and functional materials. We and others recently used CNFs to prepare transparent nanopapers,[11] bioinspired nanocomposites[12] and fibers[13] with excellent mechanical and functional properties.[14]

Moreover, CNF hydrogels are interesting for biomaterials and fundamental cell studies as they offer a stiff nanofibrillar microenvironment for cells and complement polymeric hydrogels.[15] Reports demonstrated excellent biocompatibility,[16] successful differentiation of human mesenchymal stem cells[17] and that the pluripotency of stem cells can be maintained for extended times.[18] Additionally, transparent nanopapers are emerging as gas-impermeable substrates for transient, biodegradable electronics.[11d,19] For both applications, it is important to find approaches towards gradient films. On the one hand to enable an understanding of material/cell interactions. On the other hand, to engineer strain fields of nanopapers, so that printed circuitry can be located on stiff, non-deformable parts, while mechanical stress can be dissipated in stretchy areas.

[*] B. Wang, A. J. Benitez, F. Lossada, Dr. R. Merindol, Dr. A. Walther
DWI—Leibniz Institute for Interactive Materials
Forckenbeckstr. 50, 52056 Aachen (Germany)
E-mail: walther@dwi.rwth-aachen.de
Homepage: http://www.dwi.rwth-aachen.de

Supporting information for this article can be found under: http://dx.doi.org/10.1002/anie.201511512.

Towards gradient nanocellulose materials, a first approach recently showed a patterned polymer hydrogel reinforced with cellulose nanocrystals, obtained via different crosslinking times at various positions.[20] However, patterned or highly reinforced bulk materials, complex patterns, and the use of CNFs have not been reported. Moreover, the characterization of mechanical properties remained relatively superficial, calling for detailed in situ techniques to learn more about the effect of gradient slopes on mechanical deformation behavior and strain fields.

Here we show a facile approach to prepare bulk gradient nanocomposites of CNFs and a tailor-made synthetic copolymer, which is designed to allow maximum energy dissipation and increased toughness in bioinspired nanocomposite settings. We exploit the shear-thinning nature of CNF hydrogels to first write filaments of CNF/polymer hydrogels of different composition next to each other in stripe patterns. Subsequent self-healing of the hydrogels during drying leads to coherent films, that contain the pattern information encoded via the filament writing. Although we use a manual direct filament writing for proof-of-concept purposes at this point, the process can be fully automated in future. The overall strategy presents a new approach towards merging top-down and bottom-up structuring, which becomes of increasing importance for emerging 4D printing of multiscale and heterostructured materials with anisotropic response to external fields.[21]

The detailed preparation of the gradient films is sketched in Scheme 1. First, anionic CNFs (diameter ca. 2 nm; length up to 3 μm; 0.44 mmol g^{-1} COOH groups; AFM in Figure S1) are mixed with a rationally designed copolymer in the respective weight ratios of 90/10–20/80. The total concentration of the components is adjusted according to the estimated bulk densities of the CNF (ca. 1.35 g mL^{-1}) and the polymer (ca. 1 g mL^{-1}), so as to minimize thickness differences in the bulk films after extrusion and drying. The total concentrations center around 1.3 wt % to assure a hydrogel state and minimize flow and diffusion during the "healing" of the extruded filaments into a film.

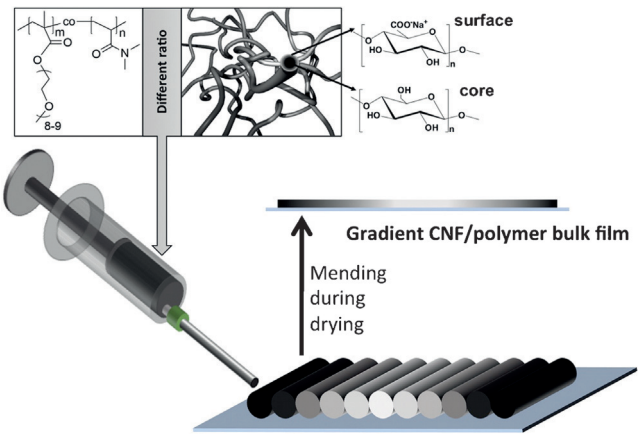

Scheme 1. Gradient CNF/polymer nanocomposites via direct filament writing of composite hydrogels and subsequent "healing" of the hydrogel filaments during drying to form a mechanically coherent bulk film.

The copolymer is a fully water-soluble poly[(ethylene glycol methyl ether methacrylate)-*co*-*N*,*N*-dimethylacrylamide] copolymer (EG-*co*-DMA), prepared by free radical copolymerization. It is tuned in its composition (54/46 molar ratio) to an optimum glass transition temperature ($T_g = 26\,°C$) and to a high apparent weight-average molecular weight ($M_w = 2.3$ MDa, $Đ \approx 1.3$) to allow high inelastic deformation in CNF/polymer nanopapers. Furthermore, it is designed to be a highly hydrophilic, but non-ionic polymer, so that it can be mixed with anionic CNFs without coagulation in water to prevent ill-defined structure formation[11a] and poor predictability of mechanical behavior. Once the water is evaporated, firm hydrogen-bonding in bulk allows for tight cohesion and efficient stress transfer.[22]

The suitability of EG-*co*-DMA to modulate the mechanical properties in CNF composite nanopapers can be derived from tensile tests of nanopapers with different fractions of CNF/EG-*co*-DMA (Figure 1 a,b). A substantial toughening occurs upon increasing the fraction of the soft, energy-dissipating EG-*co*-DMA copolymer. The elongation at break, ε_{max}, increases by 500 %, while the stiffness, E, drops from above 15 GPa to below 1 GPa upon changing from pure CNF to CNF/EG-*co*-DMA = 20/80. These changes are brought about by the homogeneous incorporation of the polymer between the nanofibrils, which replaces strong interfibrillar CNF/CNF bonding by CNF/polymer hydrogen-bonded contacts.[22] This in turn mediates the frictional sliding of the CNFs during deformation, due to the appropriate adjustment of the T_g in EG-*co*-DMA. This adjustability of the mechanical behavior of CNF/polymer nanopapers is itself a noteworthy result, because predictable toughening has so far been mainly achieved upon mixing of CNFs with structurally analogous polysaccharides[23] and added plasticizers,[24] whereas CNF hybrids with synthetic polymers[12d] often showed singularities in mechanical behavior and rather poor predictability. Overall, the designed copolymer enables a wide and desirable tunability in terms of mechanical properties.

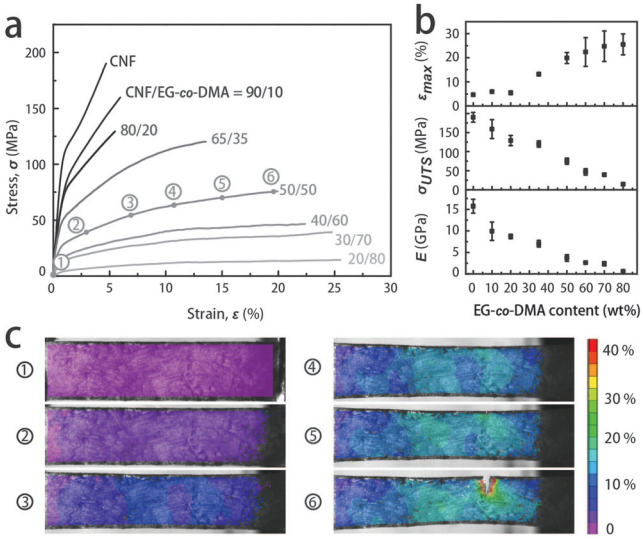

Figure 1. Toughened CNF/EG-*co*-DMA hybrid nanopapers. a,b) Mechanical properties, and c) DIC strain fields of CNF/EG-*co*-DMA = 50/50 during tensile testing at the positions indicated in the stress-strain curve. The color code indicated the local strain.

To clearly understand mechanical gradient materials, it is important to develop direct in situ methods that are able to visualize deformation mechanisms with high spatial and temporal resolution. To this end, we use digital image correlation (DIC) to investigate tensile specimens covered with a stochastic speckle pattern of black laser printer ink. DIC computes the local displacements of the speckles against each other and establishes strain fields with high spatiotemporal resolution. We first apply DIC to a strongly toughened CNF/EG-*co*-DMA = 50/50 hybrid nanopaper. The corresponding strain maps show a homogeneous evolution till around 10% strain, while thereafter a necking phenomenon reminiscent of plastic materials occurs. This leads to a preferred localization of the strain on the right hand side (Figure 1c). Finally, a crack nucleates and migrates through the whole sample with high local strain in the process zone around the crack tip. Importantly, the localization of the necking and the final crack are uncontrollable in homogeneous materials, and ultimately driven by defects. Overall this measurement serves as a basic reference, exemplifying the evolution of strain fields in a homogeneous, strongly toughened nanopaper.

Next, we discuss the basic characterization of the gradient films prepared via sequential direct writing. The width of a slice of the gradient films can be adjusted via the diameter or geometry of the extrusion needle. We focus on films prepared by extrusion through small needles with 2–3 mm diameter to investigate small scale patterning and the accuracy of the method. The confidence of the preparation can be followed by FTIR measurements at different positions of the samples, and correlating them with the spectra of homogeneous nanocomposites. Figure 2b depicts the FTIR spectra for pure CNF and EG-*co*-DMA, as well as for selected CNF/EG-*co*-DMA nanopapers. The main changes are observed at 1725 cm^{-1} and 3336 cm^{-1}, which correspond to the C=O stretching vibration of the ester bond in EG-*co*-DMA, and the O-H stretching vibration of CNFs, respectively. Minor changes are observed in the range of 1550 to 1680 cm^{-1}.

Based on the two dominant changes, it is possible to approximate a relation between their ratio, y, ($I_{\text{EG-}co\text{-DMA}}$ at 1725 cm^{-1}; I_{CNF} at 3336 cm^{-1})

$$y = \frac{I_{\text{CNF}}}{I_{\text{EG}-co-\text{DMA}}} = \frac{I_{3336\ \text{cm}^{-1}}}{I_{1725\ \text{cm}^{-1}}} \tag{1}$$

and the mass compositions, z, (X_{CNF} and $X_{\text{EG-}co\text{-DMA}}$)

$$z = \frac{X_{\text{CNF}}}{X_{\text{EG}-co-\text{DMA}}} \tag{2}$$

via a linear fit using a and b as constants (Figure 2c).

$$y = \frac{I_{\text{CNF}}}{I_{\text{EG}-co-\text{DMA}}} = az + b = a\frac{X_{\text{CNF}}}{X_{\text{EG}-co-\text{DMA}}} + \text{b} \tag{3}$$

Rearrangement according to the weight fractions delivers an expression to calculate the actual weight fractions from the intensity ratios of both peaks, y.

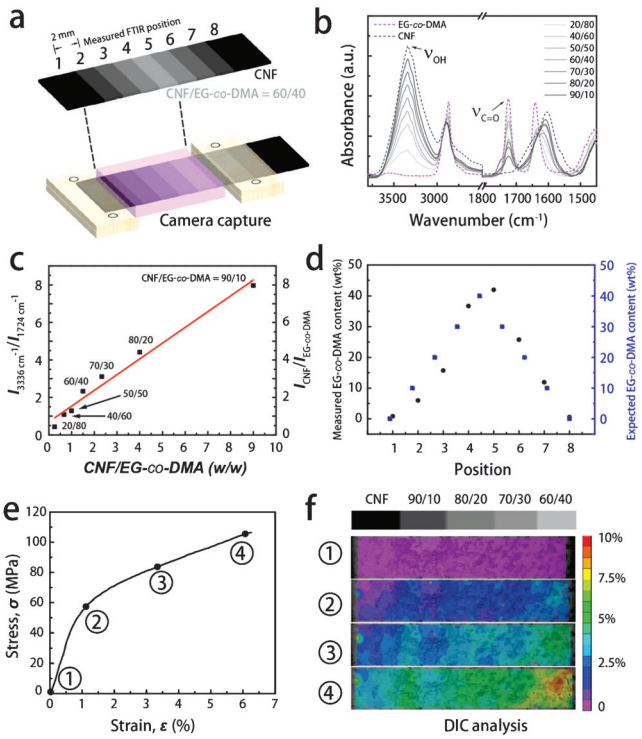

Figure 2. Characterization of gradient hybrid nanopapers. a) Scheme for a parabolic gradient and its actual visualization in the DIC tensile test setup. b,c) FTIR spectra for homogeneous CNF/EG-*co*-DMA nanopapers, and the calibration curve to determine the spatial distribution of both components from point-wise FTIR measurements. d) Comparison of the expected and calculated composition of the parabolic gradient shown in (a). e,f) Stress/strain curve and DIC patterns at the respective part of the film shown in (a).

$$\frac{X_{\text{CNF}}}{X_{\text{EG}-co-\text{DMA}}} = \frac{\frac{I_{\text{CNF}}}{I_{\text{EG}-co-\text{DMA}}} - b}{a} \tag{4}$$

Note that the fit line does not pass through zero because the FTIR peaks contain small signals of the other components.

We exemplify the use of this calibration for an extensive parabolic gradient film made by sideways direct writing of CNF/EG-*co*-DMA = 100/0, 90/10, 80/20, 70/30, 60/40, 70/30, 80/20, 90/10 and 0/100 using a 2 mm needle. Indeed, the point-wise FITR analysis (spaced by 2 mm, Figure 2a) and correlation with the calibration curves allows concluding that the calculated compositions agree well with the targeted ones (Figure 2d). This demonstrate that excess diffusion and mixing is absent during the drying, and that the stepwise fabrication reliably generates defined gradient films with mm-scale variations in composition.

Corresponding to this compositional analysis, we describe the DIC analysis during tensile testing. Due to size restrictions in the DIC measurement setup—a compromise between microscope, resolution and tensile tester—the corresponding DIC analyses can only be performed across one half of the specimen (1 cm length, 2.25 mm width), hence from pure CNF to CNF/EG-*co*-DMA = 60/40. The resolution of the DIC map is ca. 10 μm^2/pixel. Note that we chose this particular sample to be composed of the stiffer and stronger

compositions of all available nanocomposites (CNF > 60 wt %; Figure 1 a) to prevent any ambiguities from necking phenomena occurring in samples with strong plastic deformation (Figure 1 c). This allows to clearly assign the changes in the strain field to compositional variations. As expected, we find a continuous increase in the relative strain from low deformation on the left to high relative deformation on the right (Figure 2 f). The right hand side typically has 2–3 times of the local strain compared to left. The continuously increasing strain fields also reveal that the mending of the hydrogel filaments during drying delivers a strong mechanical cohesion between the various written hydrogel filaments, as fracture or stress concentration along the filament boundaries are absent. Additionally, it is important to point out that the corresponding tensile curve (Figure 2 e) is different from the ones of the homogeneous nanocomposites above (Figure 1 a,b). This is expected because the deformation is focused differently in specific areas, and does not act on the full specimen anymore. Hence, failure must occur at earlier global strain (< 6 %) compared to the most ductile pure composite nanopaper used for the preparation of the gradient (CNF/EG-*co*-DMA = 60/40; Figure 1 b). Yet, the local strain in the toughened area is substantially higher (10 %) and is in range with the most ductile composition.

Consequently, since the focus in this study lies on the modulation of the deformation patterns, we highlight in the following instructive possibilities to engineer strain fields using appropriate material combinations, without a further correlation to global tensile testing curves. To this end, we now focus on parabolic strain fields prepared via symmetric deposition of CNF/EG-*co*-DMA compositions from high-to-low-to-high content of CNF (Figure 3 a,c,d).

First, it is interesting to compare the linear gradient from above (Figure 2 f) to the parabolic gradient in Figure 3 a regarding the influence of the gradient step height on the strain field localization. The comparison shows that larger step heights from stiff and strong compositions (90/10) to ductile ones (50/50) lead to a much stronger focusing of the deformation within the soft parts (Figure 3 a). This strong focusing again demonstrates that a strong cohesion develops between the filaments during drying as stress does not excessively concentrate at the interface between hard and soft materials. From a further comparison of the strain fields of the various parabolic gradients (Figure 3 a,c,d), one can infer that the parabolic profile can be modulated to have a higher width (lower gradient) and a higher depth (more strain) for gradients of increasingly smaller steps and for a central material with highest content of toughening EG-*co*-DMA, respectively. This is evident by looking at the total strain in the center parts of the sample series, which increases from a-c-d from 20 % to 32 % maximum strain. Similarly, in all cases, the stiffest parts, clamped at the outer sides, undergo hardly any deformation.

Finally, to further showcase the possibilities and precision of the strain field engineering, we display an alternating Zebra pattern, in which hard (70/30) and soft (50/50) CNF/EG-*co*-DMA hybrid nanopapers alternate to give an oscillating deformation map (Figure 3 b). The very high sensitivity of DIC reveals some imperfections when comparing patches of

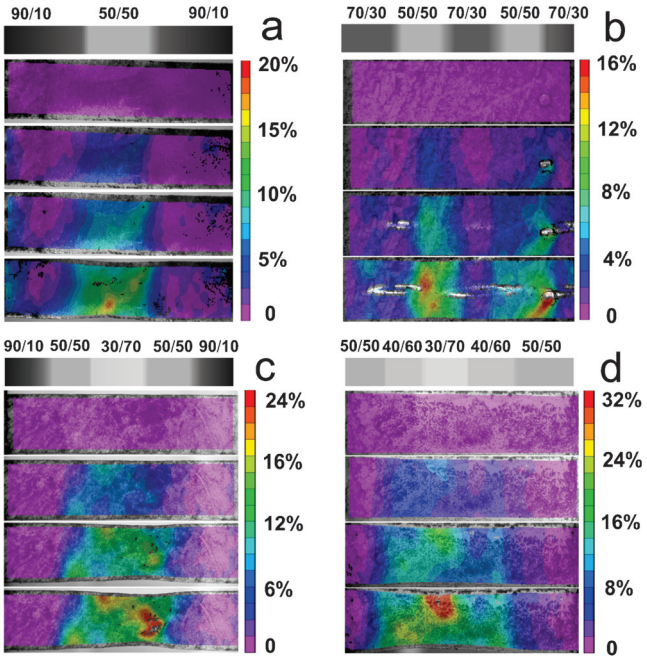

Figure 3. Modulation of strain maps. a,c,d) parabolic central gradients, and b) an alternating pattern (light reflection in the DIC map of (b) is caused by buckling of hard/soft alternating patterns). The images in each panel are arranged from top to bottom for increasing global deformation, with the lowest image just before fracture (see also Figure 1 e).

the same softness during in situ testing. These are however in a reasonable range considering that the total length of the specimen is only 1 cm, and that we target high-resolution patterns at small length scales. We believe that those defects can be alleviated using fully automated filament printers. All of the parabolic gradients clearly demonstrate how strain energy can be localized and controllably dissipated in specific sections of the nanopapers by careful orchestration of the sequential fabrication process using different nanopaper compositions. As an important consequence, fracture in these nanopapers is no longer a defect-driven process, but can now be controlled to occur in the softest parts by design.

In conclusion, we presented a conceptual approach to make desirable, bioinspired, mechanical, gradient nanocomposites by merging a top-down additive fabrication method, direct filament writing, with tailor-made nanocomposites of emerging renewable CNFs toughened by the addition of a rationally designed copolymer in a bottom-up way. This contributes a new design approach to future 4D printing—an emerging topical area at the interface of chemistry and materials science. The elastic properties and the ductility of the individual nanopaper compositions can be modulated by one order of magnitude by changing the ratios of both components. The key features to prepare well-defined gradient materials are the shear-thinning behavior of the hydrogels and their self-healing nature allowing a defined writing and subsequent mending of the filaments into continuous films. The developed routines permit to prepare gradient materials down to millimeter-scale features, and incorporating linear, parabolic or oscillating patterns. We

suggest that the process can be automated and even extended to 3D gradients by deposition of layered structures. The developed DIC routine can visualize the corresponding strain fields with submillimeter resolution. Moreover, DIC is of high importance for an in-depth characterization of the asymmetry of strain fields, and enables to understand how gradient step heights influence the ability for mechanical deformation, which cannot be inferred by looking at the global tensile behavior alone. We envisage such gradients to be relevant for fundamental studies towards the interaction of cells with CNF materials, as advanced mechanical materials with higher toughness, for complex origami actuators, as well as for strain-engineered substrates for printed electronics that maintain intact and operational even at high global deformation.

Acknowledgements

We thank the BMBF for the Aquamat Research Group and the CSC for a scholarship of B.W.

Keywords: 3D printing · bioinspired nanocomposites · gradient materials · nanocellulose · self-assembly

How to cite: *Angew. Chem. Int. Ed.* **2016**, *55*, 5966–5970
Angew. Chem. **2016**, *128*, 6070–6074

[1] A. Miserez, T. Schneberk, C. Sun, F. W. Zok, J. H. Waite, *Science* **2008**, *319*, 1816–1819.
[2] a) J. H. Waite, H. C. Lichtenegger, G. D. Stucky, P. Hansma, *Biochemistry* **2004**, *43*, 7653–7662; b) S. Suresh, *Science* **2001**, *292*, 2447–2451.
[3] L. Wang, Y. Li, G. Huang, X. Zhang, B. Pingguan-Murphy, B. Gao, T. J. Lu, F. Xu, *Crit. Rev. Biotechnol.* **2015**, *0*, 1–13.
[4] a) R. Libanori, R. M. Erb, A. Reiser, H. Le Ferrand, M. J. Süess, R. Spolenak, A. R. Studart, *Nat. Commun.* **2012**, *3*, 1265; b) L. Ionov, *Mater. Today* **2014**, *17*, 494–503; c) K. U. Claussen, T. Scheibel, H.-W. Schmidt, R. Giesa, *Macromol. Mater. Eng.* **2012**, *297*, 938–957.
[5] D. Kokkinis, M. Schaffner, A. R. Studart, *Nat. Commun.* **2015**, *6*, 8643.
[6] K. U. Claussen, R. Giesa, H.-W. Schmidt, *Polymer* **2014**, *55*, 29–38.
[7] K. U. Claussen, E. S. Lintz, R. Giesa, H.-W. Schmidt, T. Scheibel, *Macromol. Biosci.* **2013**, *13*, 1396–1403.
[8] V. E. G. Diederich, P. Studer, A. Kern, M. Lattuada, G. Storti, R. I. Sharma, J. G. Snedeker, M. Morbidelli, *Biotechnol. Bioeng.* **2013**, *110*, 1508–1519.
[9] D. Klemm, F. Kramer, S. Moritz, T. Lindström, M. Ankerfors, D. Gray, A. Dorris, *Angew. Chem. Int. Ed.* **2011**, *50*, 5438–5466; *Angew. Chem.* **2011**, *123*, 5550–5580.
[10] a) T. Saito, S. Kimura, Y. Nishiyama, A. Isogai, *Biomacromolecules* **2007**, *8*, 2485–2491; b) A. Isogai, T. Saito, H. Fukuzumi, *Nanoscale* **2011**, *3*, 71–85; c) T. Saito, Y. Nishiyama, J.-L. Putaux, M. Vignon, A. Isogai, *Biomacromolecules* **2006**, *7*, 1687–1691; d) M. Pääkkö, M. Ankerfors, H. Kosonen, A. Nykänen, S. Ahola, M. Österberg, J. Ruokolainen, J. Laine, P. T. Larsson, O. Ikkala, T. Lindström, *Biomacromolecules* **2007**, *8*, 1934–1941; e) S. Iwamoto, W. Kai, A. Isogai, T. Iwata, *Biomacromolecules* **2009**, *10*, 2571–2576; f) A. Šturcová, G. R. Davies, S. J. Eichhorn, *Biomacromolecules* **2005**, *6*, 1055–1061.
[11] a) A. J. Benítez, J. G. Torres-Rendon, M. Poutanen, A. Walther, *Biomacromolecules* **2013**, *14*, 4497–4506; b) H. Sehaqui, Q. Zhou, O. Ikkala, L. A. Berglund, *Biomacromolecules* **2011**, *12*, 3638–3644; c) M. Nogi, S. Iwamoto, A. N. Nakagaito, H. Yano, *Adv. Mater.* **2009**, *21*, 1595–1598; d) H. Fukuzumi, T. Saito, T. Iwata, Y. Kumamoto, A. Isogai, *Biomacromolecules* **2009**, *10*, 162–165.
[12] a) C.-N. Wu, T. Saito, S. Fujisawa, H. Fukuzumi, A. Isogai, *Biomacromolecules* **2012**, *13*, 1927–1932; b) A. Liu, A. Walther, O. Ikkala, L. Belova, L. A. Berglund, *Biomacromolecules* **2011**, *12*, 633–641; c) P. Laaksonen, A. Walther, J.-M. Malho, M. Kainlauri, O. Ikkala, M. B. Linder, *Angew. Chem. Int. Ed.* **2011**, *50*, 8688–8691; *Angew. Chem.* **2011**, *123*, 8847–8850; d) M. Wang, A. Olszewska, A. Walther, J.-M. Malho, F. H. Schacher, J. Ruokolainen, M. Ankerfors, J. Laine, L. A. Berglund, M. Österberg, O. Ikkala, *Biomacromolecules* **2011**, *12*, 2074–2081.
[13] a) J. G. Torres-Rendon, F. H. Schacher, S. Ifuku, A. Walther, *Biomacromolecules* **2014**, *15*, 2709–2717; b) P. Das, T. Heuser, A. Wolf, B. Zhu, D. E. Demco, S. Ifuku, A. Walther, *Biomacromolecules* **2012**, *13*, 4205–4212; c) A. Walther, J. V. I. Timonen, I. Díez, A. Laukkanen, O. Ikkala, *Adv. Mater.* **2011**, *23*, 2924–2928.
[14] M. Wang, I. V. Anoshkin, A. G. Nasibulin, J. T. Korhonen, J. Seitsonen, J. Pere, E. I. Kauppinen, R. H. A. Ras, O. Ikkala, *Adv. Mater.* **2013**, *25*, 2428–2432.
[15] a) A. J. Engler, S. Sen, H. L. Sweeney, D. E. Discher, *Cell* **2006**, *126*, 677–689; b) E.-R. Janeček, J. R. McKee, C. S. Y. Tan, A. Nykänen, M. Kettunen, J. Laine, O. Ikkala, O. A. Scherman, *Angew. Chem. Int. Ed.* **2015**, *54*, 5383–5388; *Angew. Chem.* **2015**, *127*, 5473–5478; c) J.-M. Malho, S. Arola, P. Laaksonen, G. R. Szilvay, O. Ikkala, M. B. Linder, *Angew. Chem. Int. Ed.* **2015**, *54*, 12025–12028; *Angew. Chem.* **2015**, *127*, 12193–12196.
[16] a) M. Bhattacharya, M. M. Malinen, P. Lauren, Y.-R. Lou, S. W. Kuisma, L. Kanninen, M. Lille, A. Corlu, C. GuGuen-Guillouzo, O. Ikkala, A. Laukkanen, A. Urtti, M. Yliperttula, *J. Control. Release* **2012**, *164*, 291–298; b) M. M. Malinen, L. K. Kanninen, A. Corlu, H. M. Isoniemi, Y.-R. Lou, M. L. Yliperttula, A. O. Urtti, *Biomaterials* **2014**, *35*, 5110–5121; d) J. G. Torres-Rendon, M. Kopf, D. Gehlen, A. Blaeser, H. Fischer, L. DeLaporte, A. Walther, *Biomacromolecules*, **2016**, *17*, 905–913.
[17] J. G. Torres-Rendon, T. Femmer, L. De Laporte, T. Tigges, K. Rahimi, F. Gremse, S. Zafarnia, W. Lederle, S. Ifuku, M. Wessling, J. G. Hardy, A. Walther, *Adv. Mater.* **2015**, *27*, 2989–2995.
[18] Y.-R. Lou, L. Kanninen, T. Kuisma, J. Niklander, L. A. Noon, D. Burks, A. Urtti, M. Yliperttula, *Stem Cells Dev.* **2013**, *23*, 380–392.
[19] a) Y. H. Jung, T.-H. Chang, H. Zhang, C. Yao, Q. Zheng, V. W. Yang, H. Mi, M. Kim, S. J. Cho, D.-W. Park, H. Jiang, J. Lee, Y. Qiu, W. Zhou, Z. Cai, S. Gong, Z. Ma, *Nat. Commun.* **2015**, *6*, 7170; b) J. Huang, H. Zhu, Y. Chen, C. Preston, K. Rohrbach, J. Cumings, L. Hu, *ACS Nano* **2013**, *7*, 2106–2113.
[20] J. D. Fox, J. R. Capadona, P. D. Marasco, S. J. Rowan, *J. Am. Chem. Soc.* **2013**, *135*, 5167–5174.
[21] J. Choi, O. C. Kwon, W. Jo, H. J. Lee, M.-W. Moon, *3D Print. Addit. Manuf.* **2015**, *2*, 159–167.
[22] a) X. Xu, F. Liu, L. Jiang, J. Y. Zhu, D. Haagenson, D. P. Wiesenborn, *ACS Appl. Mater. Interfaces* **2013**, *5*, 2999–3009; b) T. Kondo, C. Sawatari, R. S. J. Manley, D. G. Gray, *Macromolecules* **1994**, *27*, 210–215; c) T. Aoki, M. Kawashima, H. Katono, K. Sanui, N. Ogata, T. Okano, Y. Sakurai, *Macromolecules* **1994**, *27*, 947–952.
[23] H. Sehaqui, Q. Zhou, L. A. Berglund, *Soft Matter* **2011**, *7*, 7342–7350.
[24] A. J. Svagan, M. A. S. Azizi Samir, L. A. Berglund, *Biomacromolecules* **2007**, *8*, 2556–2563.

Received: December 11, 2015
Revised: January 29, 2016
Published online: April 8, 2016

